Published in final edited form as:
Biochemistry. 2008 November 25; 47(47): 12389–12397. doi:10.1021/bi801491e.

Substrate-Ligand Interactions in *Geobacillus Stearothermophilus* Nitric Oxide Synthase†

Mariam Kabir[1], **Jawahar Sudhamsu**[2], **Brian R. Crane**[2], **Syun-Ru Yeh**[*,1], and **Denis L. Rousseau**[*,1]

[1]Department of Physiology and Biophysics, Albert Einstein College of Medicine, Bronx, NY 10461

[2]Department of Chemistry and Chemical Biology, Cornell University, Ithaca NY 14853

Abstract

Ntric oxide synthase (NOS) generates NO via a sequential two-step reaction, L-arginine (L-Arg) → N-hydroxy-L-arginine (NOHA) → L-citrulline + NO. Each step of the reaction follows a distinct mechanism defined by the chemical environment introduced by each substrate bound to the heme active site. The dioxygen complex of the NOS enzyme from a thermophilic bacterium, *Geobacillus stearothermophilus* (gsNOS), is unusually stable; hence it provides a unique model for the studies of the mechanistic differences between the two steps of the NOS reaction. By using CO as a structural probe, it was found that gsNOS exhibits two conformations in the absence of substrate, as indicated by the presence of two sets of the $\nu_{Fe\text{-}CO}/\nu_{C\text{-}O}$ modes in the resonance Raman spectra. In the $\nu_{Fe\text{-}CO}$ versus $\nu_{C\text{-}O}$ inverse correlation plot, one set of the data falls on the correlation line characterized by mammalian NOSs (mNOS), whereas the other set of the data lies on a new correlation line defined by a bacterial NOS from *Bacillus subtilis* (bsNOS), reflecting a difference in the proximal Fe-Cys bond strength in the two conformers of gsNOS. The addition of L-Arg stabilizes the conformer associated with the mNOS correlation line, whereas NOHA stabilizes the conformer associated with the bsNOS correlation line, although both substrates introduce a positive electrostatic potential to the distal heme pocket. To assess how substrate-binding affects the Fe-Cys bond strength, the frequency of the Fe-Cys stretching mode of gsNOS was monitored by resonance Raman spectroscopy with 363.8 nm excitation. In the substrate-free form, the Fe-Cys stretching mode was detected at 342.5 cm^{-1} similar to that of bsNOS. The binding of L-Arg and NOHA brings about a small decrease and increase in the Fe-Cys stretching frequency, respectively. The implication of these unique structural features on the oxygen chemistry of NOS is discussed.

Keywords

Nitric Oxide; Raman Scattering; Biophysics; Carbon Monoxide

Mammalian nitric oxide synthase (mNOS) produces NO via a sequential two-step reaction. (1) In the first step of the reaction, L-Arg is oxidized to N-hydroxy-L-arginine (NOHA), with the consumption of two electrons and one molecule of oxygen. In the second step,

†This work was supported by grants from the NIH (GM054806 to DLR) and from the NSF (CHE-0749997 to BRC). MK is supported by the Medical Scientist Training Program at the Albert Einstein College of Medicine (NIH GM08572).

*CORRESPONDING AUTHORS: Syun-Ru Yeh: syeh@aecom.yu.edu, Tel. (718) 430-4234, Fax. (718) 430-4230; or Denis Rousseau: rousseau@aecom.yu.edu, Tel. (718) 430-4264, Fax. (718) 430-8808 .

Supporting Information Available. The absence of significant differences resulting from the addition of H4B on the optical spectra (Fig. 1S), the resonance Raman spectra of the CO adducts (Fig. 2S) and the resonance Raman spectra of the Fe-Cys stretching mode (Fig. 3S) are included in the Supplementary Data. This material is available free of charge on the internet at http://pubs.acs.org.

NOHA is further oxidized to L-citrulline and NO, by using an additional electron and another molecule of oxygen as illustrated in Scheme 1. The three major isoforms of mNOS present in macrophages (iNOS), endothelial cells (eNOS) and neuronal tissues (nNOS), produce NO that functions as a cytotoxic agent, a vasodilator, and a neurotransmitter, respectively. All three isoforms of mNOS consist of a reductase domain with NADPH, FAD and FMN binding sites, and an oxygenase domain, containing tetrahydrobiopterin (H4B), heme and the substrate binding site.(1) The mNOS enzymes function as a dimer, and, during the reaction, electron travels from the NADPH, FAD to FMN in the reductase domain of one subunit, culminating in the heme iron of the oxygenase domain of the other subunit, where the oxygen reaction takes place(2). Calcium/calmodulin binding enables electron transfer between the two domains.(3)

Although the full-length mNOS enzymes have not been crystallized, the structures of the oxygenase domains of all three mammalian isoforms ($mNOS_{oxy}$) have been solved and found to be nearly identical.(4-9) It is important to note that the oxygenase domain of mNOS ($mNOS_{oxy}$) is fully functional in the presence of the substrate and cofactor *in vitro*, when an electron source is available.(10) As illustrated in Fig. 1B and 1C, using the crystal structures of $iNOS_{oxy}$ as an example, the substrate binds directly over the heme iron, consistent with the prediction made by a variety of spectroscopic studies.(11-15) The binding is stabilized by an H-bonding network involving Glu371, Trp366 and Tyr367, as well as one of the two heme propionate groups and H4B. As a member of the P450 family of enzymes, the heme iron in NOS is coordinated by a cysteine residue (Cys194 in iNOS) as the proximal ligand. Nonetheless, distinct from P450, in which the proximal cysteine-thiolate ligand is H-bonded to three backbone amino groups, the proximal cysteine ligand of mNOS accepts an H-bond from a nearby Trp residue side-chain (Trp188 in iNOS),(16-20) in addition to two H-bonds from backbone amino groups. The Trp-Cys H-bond is believed to be important in regulating the electron density on the heme iron for the oxygen chemistry. (16-19, 21)

In addition to mammals, genes coding for NOS-like enzymes have been found in several other organisms, including bacteria. Seven bacterial NOSs, including those from *Streptomyces turgidiscabies*(22), *Nocardia sp.*(23), *Deinococus radiodurans*(24), *Bacillus subtilis* (bsNOS)(25), *Bacillus anthracis*(26), *Staphylococcus aureous* (saNOS)(27) and *Geobacillus stearothermophilus* (gsNOS)(28), have been expressed and partially characterized. Among them, bsNOS,(29) saNOS,(30) and gsNOS,(28) have been crystallized. The structures of the three bacterial NOSs are very similar. They exhibit characteristics resembling those of $mNOS_{oxy}$ (see Fig. 1A vs 1B), except that the bacterial NOSs lack a portion of the cofactor binding site, as well as the N-terminal hook, which links the two subunits of the dimer together(5) and the associated Zn-binding site. Although these two structural features have been recognized to be important in the formation of the dimer interface in mNOS,(31) their absence in bacterial NOS does not seem to compromise their ability to form dimers. On the contrary, the dimeric interactions in the bacterial NOS are as strong as their mammalian counterparts.(29)

Although the overall crystallographic structures of the bacterial NOSs and $mNOS_{oxy}$ are similar, distinct solution structural properties have been revealed by a variety of spectroscopic studies as summarized by Salard *et al.*(26) For example, on the basis of optical absorption measurements(26) the heme iron in the substrate and cofactor-free ferric derivative of saNOS has either a six-coordinate (6C) low-spin or a high-spin/low-spin mixed electronic configuration, like that observed in the mNOSs, indicating a water molecule is coordinated to the heme iron on the distal side, whereas that in bsNOS is five-coordinate (5C) high-spin, suggesting that the water molecule is destabilized in the distal ligand binding site. On the other hand, resonance Raman studies of the CO-adducts of both bsNOS(27) and

saNOS(25) revealed two Fe-CO stretching modes ($\nu_{Fe\text{-}CO}$) in the 480-500 cm^{-1} region, corresponding to two possible conformers of the Fe-CO moiety. Like the bacterial enzymes, in iNOS two conformers were detected; (32) whereas in nNOS three conformers were reported (32, 33). In addition, L-Arg binding in the bacterial NOSs causes the merging of the two $\nu_{Fe\text{-}CO}$ modes into a single mode at ~502-504 cm^{-1}, similar to the frequency observed in nNOS, but distinct from that of iNOS and eNOS (in which the mode is located at ~512 cm^{-1}).(14) In contrast to bsNOS and saNOS, until now no resonance Raman studies have been reported for the NOS from *Geobacillus stearothermophilus*.

Geobacillus stearothermophilus is a thermophilic bacterium found in warm compost. It lives optimally between 43 and 75°C, and as such the turnover rate of gsNOS is slower at room temperature as compared to other members of the NOS family.(28) Furthermore, the decay rate of the primary dioxygen-bound intermediate of gsNOS has been found to be ~10-fold slower than that of other NOS enzymes.(28) Although some relatively minor structural differences in the distal heme pocket of gsNOS have been noted as compared to $mNOS_{oxy}$, (28) the heme active sites of the NOSs are nearly superimposable (see Fig. 1A and B),(28) and there are no obvious structural features that may account for the enhanced stability of the dioxygen-complex of gsNOS.

The understanding of the catalytic mechanism of the NOS enzymes has been hampered by the fact that no oxygen-containing intermediates other than the primary dioxygen-complex have been well-characterized during the reaction cycle. Nonetheless, on the basis of various spectroscopic studies,(32, 34-37) it is generally believed the first step of the NOS reaction, L-Arg → NOHA, follows the P450-type of mechanism, in which the active oxygen species is a Compound I-type ferryl intermediate;(32, 34, 36) whereas the second step of the reaction, NOHA → L-citrulline + NO, follows the heme oxygenase type of chemistry, where the active oxygen species is a peroxyl intermediate.(32, 37) The difference in the catalytic mechanisms of the two steps of the NOS reaction indicates that L-Arg and NOHA interact differently with the heme-bound dioxygen in the catalytic site of NOS, thereby dictating the mechanism by which the oxygen chemistry proceeds. The nature of the interaction between the substrates and heme-bound ligand in NOS may be studied by using CO as a structural probe. With this approach, the isoform-specific substrate-ligand interactions in $mNOS_{oxy}$ have been identified(14) and the differing interactions between the substrates and the catalytic pockets have been examined.(13, 21, 32, 38) In the present work, optical absorption and resonance Raman spectroscopies were used to study various derivatives of gsNOS in the absence and presence of substrate (either L-Arg or NOHA) and cofactor (H4B). The results are compared to those of mNOSs as well as other bacterial NOSs, and discussed in the context of oxygen chemistry in NOS.

Materials and Methods

(6*R*)-5,6,7,8-tetrahydro-$_L$-biopterin was purchased from Alexis Biochemicals (San Diego, CA). All other chemicals were purchased from Sigma. The isotopically labeled gas, $^{13}C^{16}O$, was supplied by Icon (Mount Marion, NY). The natural abundant gases, Ar and CO were obtained from Tech Air (White Plains, NY).

The gsNOS samples were purified in the absence of L-Arg and H4B as reported elsewhere. (28) The purified gsNOS was kept in Tris buffer (50 mM) in the presence of 150 mM NaCl at pH 7.5 and stored in liquid nitrogen until use. To generate the L-Arg/NOHA and/or H4B-bound derivatives, L-Arg/NOHA and H4B were added to the enzyme in 100-150 and 3-5 times excess with respect to the heme, respectively, and incubated at 4 °C for ~18 hrs. The binding of L-Arg and NOHA was confirmed by monitoring the optical absorption change. Although the addition of H4B did not result in any changes in the optical spectrum, the

binding of H4B, at 3-5 times excess, was confirmed by a large change in both the kinetics and thermodynamics of the decay of the primary oxy-intermediate of gsNOS in stopped-flow optical absorption measurements (unpublished data). To prepare the deoxy derivatives, the protein sample was first purged with Ar gas in a septum-sealed anaerobic cell, and reduced with sodium dithionite introduced by a gas-tight syringe. To prepare the CO derivatives, 500 μl of 1 atm of CO was injected into the deoxy samples via a gas-tight syringe. The protein concentration used for the optical absorption and resonance Raman studies was ~50 μM.

The optical absorption spectra were taken with a Shimadzu UV2100U spectrophotometer. Resonance Raman spectra were obtained by using 441.6 nm excitation from a He-Cd laser (Liconix, Santa Clara, CA) for spectra of the CO-bound adducts, and 363.8 nm excitation from an Argon ion laser (Spectra-Physics, Beamlok 2080) for spectra of the ferric form of the enzyme to enhance the Fe-Cys stretching mode. The incident laser power on the sample was kept under 3 mW. The cylindrical sample cell was rotated at ~6000 rpm during the spectral acquisition to avoid photodamage to the sample. The scattered light was collected and focused onto an entrance slit (100 μm) of a 1.25-m SPEX spectrophotometer (Jobin Yvon, Edison, NJ), and subsequently detected by a liquid nitrogen-cooled CCD (Roper Scientific, Princeton, NJ). All of the resonance Raman spectra were frequency calibrated by using spectral lines from indene, except for those in the 1800-2000 cm^{-1} spectral region, where an acetone/ferricyanide combination was used instead. Cosmic ray artifacts were removed from the spectra by using a routine in the Winspec spectral acquisition software (Roper Scientific). Most of the data were integrated for ~30 min. Longer integration times of 180 and 360 min were used to improve the signal to noise ratio for the Fe-Cys and the C-O stretching frequency regions. All measurements were made at room temperature. Optical absorption spectra were obtained before and after each resonance Raman measurement to ensure the integrity of the enzyme

RESULTS

Optical Absorption Spectroscopic Studies

Fig, 2 shows the optical absorption spectra of gsNOS in the absence of substrate and cofactor. The oxidized enzyme has a broad Soret transition at 401 nm, characteristic of a five-coordinate high-spin electronic configuration. Upon reduction, the Soret maximum shifts to ~411 nm, again indicating a five-coordinate high-spin electronic configuration, similar to that seen in other reduced NOSs.(21) The addition of CO to the ferrous enzyme causes a further shift of the Soret band to 445 nm, typical for a six-coordinate low-spin configuration of a CO-bound heme with coordination of a thiolate ligand on the proximal side. The shoulder at ~420 nm, typical of histidine coordinated CO-complexes, is attributed to the presence of a small amount of the inactive form of the enzyme commonly observable in mNOSs.(12)

The addition of L-Arg or NOHA to the ferric enzyme causes the Soret maximum to shift from 401 to 397 nm and the Soret band to be more symmetric; whereas the addition of H4B does not introduce any appreciable spectral shift (Supplementary Data: Fig. 1S). Also, both substrates cause the Soret maxima of ferrous gsNOS to shift from 411 nm to 414 nm. As in the case of ferric gsNOS, the addition of H4B does not bring about additional changes. On the other hand, the addition of substrate and/or cofactor to the CO-bound gsNOS reduces the intensity of the 420 nm band significantly without affecting the main 445 nm band, indicating the stabilization of the gsNOS structure by the binding of substrate and/or cofactor.

Resonance Raman Spectroscopic Studies of the CO-Bound Adducts

The CO-bound form of the enzyme was studied with resonance Raman spectroscopy, by using 441.6 nm excitation to probe selectively the active species associated with the Soret maximum at 445 nm. Fig 3 shows the low frequency region of the resonance Raman spectra of the CO-bound gsNOS in the absence or presence of substrate (either L-Arg or NOHA). These spectra are not affected by the addition of H4B, independent of the presence or absence of substrates (Supplementary Data: Fig. 2S).

In the absence of substrate, the broad line at ~501 cm^{-1} (left panel in Fig. 3) is assigned as the Fe-CO stretching mode ($\nu_{Fe\text{-}CO}$), which can be fitted with two Gaussian curves with peak maxima at 483 and 501 cm^{-1} (see the right panel). The small line at 562 cm^{-1} is assigned to the Fe-C-O bending mode ($\delta_{Fe\text{-}C\text{-}O}$). The assignments of these vibrational modes were confirmed by the isotope substitution of $^{12}C^{16}O$ with $^{13}C^{16}O$ (Fig. 3 and Supplementary Data: Fig. 2S). In the high frequency region of the spectra (Fig. 4), two overlapping lines at 1929 and 1952 cm^{-1} are identified as the C-O stretching modes ($\nu_{C\text{-}O}$). These data demonstrate that there are two different conformations of the Fe-CO moiety in the absence of added substrates, as reported for other members of the enzyme family.(11, 13, 14, 25, 27, 33, 38, 39)

In general, when CO binds to heme proteins, it donates electron density to the heme iron via a σ-bond to the empty d_{z2} orbital of the iron, which in turn donates electron density back to the π* orbital of the CO. Owing to the so-called "π-back-bonding" effect, CO-bound heme proteins can exist in two extreme structures:

$$Fe^{\delta-} - C \equiv O^{\delta+}\ (I) \leftrightarrow Fe{=}C{=}O\ (II) \qquad \text{eq. (1)}$$

When the distal environment is positively charged, structure II is favored over structure I. Consequently, the Fe-CO bond strength increases, resulting in an increase in the $\nu_{Fe\text{-}CO}$ stretching frequency, and the C-O bond strength decreases, resulting in a decrease in the $\nu_{C\text{-}O}$ stretching frequency.(40-42) On this basis, the $\nu_{Fe\text{-}CO}$ frequency is inversely correlated with the $\nu_{C\text{-}O}$ frequency as illustrated in Fig. 5 with the position on a given curve determined by the charge distribution in the distal heme environment. This relationship has made CO a very important probe of the distal pocket in heme proteins.

In addition to its sensitivity to the distal environment, the position of the specific $\nu_{Fe\text{-}CO}$ versus $\nu_{C\text{-}O}$ correlation line depends on the strength of the proximal-ligand bond, which determines the degree of electron donation to the heme iron, thereby modulating the π-bonding effect.(40-42) As such, the correlation line associated with heme proteins with histidine as the proximal ligand, such as hemoglobin and myoglobin, lies above that associated with heme proteins with thiolate as the proximal ligand, such as P450 (Fig. 5). Interestingly, the mNOS data points fall in-between those two correlation lines, suggesting a weaker proximal thiolate-iron bond [Fe-Cys] than that in the P450s. The weaker Fe-Cys bond in mNOS is believed to be a result of the H-bond between the proximal cysteine and a nearby Trp residue (see Fig, 1), which withdraws electron density away from the Fe-Cys bond, thereby strengthening the Fe-CO σ-bond.(13, 42, 43) Recently, Santolini *et al.* reported that the $\nu_{Fe\text{-}CO}$ versus $\nu_{C\text{-}O}$ correlation line of bsNOS(25) falls in between the mNOS and P450 lines (Fig. 5), suggesting a Fe-Cys bond stronger than that in mNOSs, but weaker than that in P450s. This conclusion is consistent with the ~5 cm^{-1} higher Fe-Cys stretching frequency ($\nu_{Fe\text{-}Cys}$) of bsNOS with respect to that of mNOS (Table 1).

The Raman data of the substrate-free (SF) gsNOS shown in Figs. 3-4 indicate the presence of two sets of $\nu_{Fe\text{-}CO}/\nu_{C\text{-}O}$ modes, one at 501/1929 cm^{-1} and the other at 483/1952 cm^{-1} (denoted as SF_1 and SF_2 in Fig. 5). Surprisingly, the SF_1 data point lies on the mNOS

correlation line, whereas the SF_2 point lies on the bsNOS correlation line (see the black circles in Fig. 5). The data suggest that, in the absence of substrate and cofactor, the two conformers of gsNOS exhibit distinct proximal as well as distal environments. This behavior is unique among the NOS family of enzymes; as may be seen in Fig. 5 all the data associated with mNOS or bsNOS fall on the same correlation line, despite that fact that conformational heterogeneity also present in these enzymes.(21)

In the presence of L-Arg, the $\nu_{Fe\text{-}CO}$ mode sharpens and shifts to 505 cm^{-1}. Curve fitting of the $\nu_{Fe\text{-}CO}$ mode revealed the presence of a weak line at 517 cm^{-1}, which is presumed to be a minor conformation of the complex. The $\nu_{C\text{-}O}$ mode associated with the major conformer is observed at 1923 cm^{-1}, whereas that associated with the minor conformer is too weak to be detected (Fig 4) and has not been analyzed further. The $\delta_{Fe\text{-}C\text{-}O}$ mode, on the other hand, shifts from 562 to 566 cm^{-1} with a significantly enhanced intensity, characteristic of a bent conformation of the Fe-C-O moiety. The $\nu_{Fe\text{-}CO}/\nu_{C\text{-}O}$ data point associated with the L-Arg-bound enzyme lies on the mNOS correlation line and shifts higher toward the left corner with respect to the SF_1 conformer of the substrate-free enzyme (Fig. 5). The data indicate that the guanidinium group of the L-Arg is in close proximity to the heme-bound CO, thereby introducing a positive electrostatic potential to the environment of the CO, and forcing the Fe-C-O moiety to adopt a bent conformation.

In the presence of NOHA, the $\nu_{Fe\text{-}CO}$ mode is detected at 493 cm^{-1} (Fig. 3). Curve fitting of the $\nu_{Fe\text{-}CO}$ band revealed the presence of a weak line at 513 cm^{-1}. The $\nu_{C\text{-}O}$ mode associated with the major conformer is observed at 1929 cm^{-1}, while that associated with the minor conformer is not visible (Fig. 4). Again, no additional analysis of the minor conformation was made. The $\delta_{Fe\text{-}C\text{-}O}$ mode slightly shifts to 561 cm^{-1}, and is significantly enhanced, indicating a bent Fe-C-O moiety. Intriguingly, the $\nu_{Fe\text{-}CO}/\nu_{C\text{-}O}$ data point associated with the NOHA-bound enzyme falls on the bsNOS correlation line and shifts higher toward the left corner with respect to the SF_2 conformer of the substrate-free enzyme (Fig. 5), again indicating that NOHA introduces a positive electrostatic potential to the surrounding of the CO.

As summarized in Table 1 and Fig. 5, the structural perturbation introduced by substrate-binding in the various members of the NOS family of enzymes are quite disparate, manifesting the possible structural features that may account for the wide spectrum of the activities associated with the various derivatives of the enzymes. The significantly enhanced $\delta_{Fe\text{-}C\text{-}O}$ in gsNOS induced by substrate-binding is unique as compared to mNOS, suggesting a congested ligand binding site in gsNOS in the presence of substrates. Taken together the data suggest that the substrate-free gsNOS exhibits structural flexibility, allowing for the coexistence of two conformers, with distinct proximal Fe-Cys strengths and distal electrostatic potentials. The binding of the substrates to gsNOS imposes structural constraints on the protein matrix, forcing the Fe-C-O moiety to adopt a bent structure and locking the enzyme in conformations with proximal Fe-Cys properties similar to those of mNOS and bsNOS for the L-Arg and NOHA-bound enzyme, respectively.

Resonance Raman Spectroscopic Studies of the Iron-Sulfur (Fe-Cys) Stretching Mode

To determine the possible role of the Fe-Cys bond strength in modulating the chemical properties of the Fe-C-O moiety, we measured the Fe-Cys stretching mode ($\nu_{Fe\text{-}Cys}$) of gsNOS in the absence or presence of L-Arg or NOHA, with and without H4B. To probe the $\nu_{Fe\text{-}Cys}$ frequency of the gsNOS, 363.8 nm excitation and the ferric enzyme was used for the resonance Raman measurements, as the $\nu_{Fe\text{-}Cys}$ mode of P450 and other NOS systems is only selectively enhanced in the ferric oxidation state with a five-coordinate high-spin electronic configuration.(25, 44-47)

A strong line in the 342-344 cm^{-1} region was identified at all conditions examined, as shown in Fig. 6. Curve fitting analysis of the data obtain in the absence of substrate shows a major line located at 342.5 cm^{-1}, and two minor lines at 350 and 375cm^{-1} assigned as intrinsic porphyrin modes. The 342.5 cm^{-1} line is assigned as the Fe-Cys stretching mode, as its intensity is dramatically enhanced with the 363.8 nm excitation as compared to the Soret excitation. Interestingly, the $\nu_{Fe\text{-}Cys}$ frequency is sensitive to substrate binding (Fig. 6), but insensitive to H4B binding (Supplementary Data: Fig. 3S). The $\nu_{Fe\text{-}Cys}$ frequency shifts from 342.5 to 342.1 and 343.3 cm^{-1} for the L-Arg and NOHA-bound enzyme, respectively. Although the shifts are small, they are confirmed by the difference spectrum shown in Fig. 6D, where the peak and trough correlate with the $\nu_{Fe\text{-}Cys}$ lines of the NOHA and L-Arg-bound enzyme, respectively. The $\nu_{Fe\text{-}Cys}$ frequencies of gsNOS are similar to that of bsNOS (~342 cm^{-1}), lower than that of P450 (~351 cm^{-1})(44-46), but higher than that of mNOS (~337 cm^{-1})(25, 47).

DISCUSSION

The data reported here demonstrate that the substrate-ligand interactions in gsNOS are quite distinct from those of the other members of the NOS family. The coexistence of two conformers of the CO-complex that lie on differing $\nu_{Fe\text{-}CO}$-$\nu_{C\text{-}O}$ correlation lines is unprecedented. It demonstrates a great deal of plasticity in the protein matrix that has functional implications. To gain an understanding of the origin of these features we consider the relationship between the strength of the Fe-Cys bond and the position of the $\nu_{Fe\text{-}CO}$ versus $\nu_{C\text{-}O}$ correlation curves as well as the factors that regulate the strength of the bond.

The Relationship between the proximal Fe-Cys bond strength and the distal Fe-C-O bond strengths

To understand how the proximal Fe-Cys bond strength affects the chemical properties of the distal Fe-C-O moiety in a quantitative fashion, the offset of the $\nu_{Fe\text{-}CO}$ versus $\nu_{C\text{-}O}$ correlation line shown in Fig. 5, as estimated by the $\nu_{Fe\text{-}CO}$ value at the $\nu_{C\text{-}O}$ = 1945 cm^{-1} point, is plotted against the $\nu_{Fe\text{-}Cys}$ frequency in Fig. 7. It was found that all the data points, except those associated with the SF_1 conformer of the substrate-free gsNOS and the L-Arg-bound gsNOS, fall on a linear line. The linear relationship confirms that the displacement of the $\nu_{Fe\text{-}CO}$-$\nu_{C\text{-}O}$ correlation lines shown in Fig. 5 is proportional to the strength of the Fe-Cys bond.

One plausible explanation for the deviation of the SF_1 and L-Arg points from the line shown in Fig. 7 is that the Fe-Cys bond strength measured in the ferric state does not necessarily reflect that associated with the CO-bound ferrous state. For example, the sensitivity of the proximal Fe-Cys bond strength to the oxidation state of the heme iron in heme-proteins has been reported for the P450 and CPO enzymes,(48) in which the Fe-Cys bond lengths are 2.23 and 2.30 Å, respectively, in the ferric high-spin states, whereas they are 2.37 Å in the ferrous oxy-complexes of both of the enzymes. It is conceivable that in the ferric form of gsNOS, the structure is locked into a conformation with a relatively strong Fe-Cys bond strength independent of the presence of the substrate, giving the relatively high frequency of the Fe-Cys mode for all of the ferric complexes. However, in the CO-complexes this conformational restraint is relieved revealing distinct substrate-dependent Fe-Cys bond strengths. Consequently, the data indicate that in the SF_1 and L-Arg bound CO-complexes of gsNOS, the Fe-Cys bond strengths are overestimated by the resonance Raman measurements of the 5C ferric states shown in Fig. 6.

Structural Features controlling the Proximal Fe-Cys bond Strength

As listed in Table 1, the Fe-Cys bond strength of the ferric NOS has the following order: $iNOS_{oxy}$ < gsNOS ~ bsNOS. In the crystallographic structure of the ferric form of gsNOS (PDB: 2FLQ,(28) Fig. 1A), the proximal Cys76 ligand accepts an H-bond from a nearby Trp70. The H-bond between Cys76 and Trp70 presumably modulates the electron donation from the Cys76 to the heme iron, thereby regulating the bond length/bond strength of the Fe-Cys moiety. Similar interactions are present in mNOS as illustrated in Fig. 1B and 1C (using iNOS as an example). The equivalent Trp residue in nNOS has been demonstrated to play a critical role in controlling the NO-binding properties of the enzyme, and consequently in regulating the NO feedback inhibition mechanism.(16-20) The Cys-Trp distance is modulated by additional H-bonding interaction(s) with the backbone carbonyl group of a nearby residue (see Gly78 and Gly 196 in gsNOS and iNOS, respectively). As listed in Table 2, the Cys-Trp distances are ~3.74 and 3.22 Å in gsNOS and $iNOS_{oxy}$, respectively. The shorter Trp-Gly distance (3.07/3.61 vs 4.71 Å) is associated with the longer Cys-Trp distance in gsNOS, resulting in a weaker Trp-Cys H-bond, and consequently a shorter Fe-Cys bond (which can not be accurately determined due to the limited resolution of the crystal structure), accounting for the higher $\nu_{Fe\text{-}Cys}$ frequency in gsNOS reported in this work.

The $\nu_{Fe\text{-}Cys}$ frequency of bsNOS, on the other hand, is similar to that of gsNOS (Table 1). However, two different Trp-Cys distances, 3.74 and 3.39Å, were observed in the two subunits of the loose-dimeric bsNOS enzyme in the absence of substrate and cofactor (PDB: 2AMO). (49) The longer distance is identical to that observed in gsNOS, suggesting that the subunit structure associated with Trp-Cys distance of 3.74 Å is the energy minimum state of bsNOS in free solution, and that the coexistence of the two conformations may be a result of the crystal packing. In the presence of THF and L-Arg (or NOHA) both subunits are identical, with Trp-Cys distances of 3.47 and 3.48 Å(29).

As shown in Fig. 5, L-Arg and NOHA binding in gsNOS induces opposite effects: the former weakens the Fe-Cys bond, whereas the latter strengthens it. As the crystal structure of the NOHA-bound gsNOS is not available, to understand how the distal substrate-protein interaction affects the proximal Fe-Cys bond strength, we compare the crystal structure of the L-Arg-bound $iNOS_{oxy}$ (Fig. 1B) to that of the NOHA-bound $iNOS_{oxy}$ (Fig. 1C). In the NOHA-bound structure, the terminal oxygen atom of the NOHA is in close proximity to a porphyrin nitrogen atom of the heme; in addition, it forms an H-bond with the backbone amine group of Gly365. These interactions, which are absent in the L-Arg-bound structure, may introduce heme distortion, which in turn may affect the position of the Trp188. As the sidechain of Trp188 engages in π-stacking with the heme, the change in its positioning would affect its H-bonding interaction with the Cys194 and thus the Fe-Cys bond strength. This hypothesis remains to be tested by additional crystallographic studies of the NOHA-bound gsNOS.

Implications in the Oxygen Chemistry of NOS

All the CO-derivatives of mNOS exhibit multiple conformations in the absence of substrates and cofactor, indicating a significant degree of conformational heterogeneity.(13, 14, 32, 38) Substrate-binding in these enzymes reduces the conformational freedom by affecting only the local interactions in the distal heme pocket, without perturbing the proximal heme environment, as indicated by the fact that all the $\nu_{Fe\text{-}CO}$-ν_{CO} data of the substrate-free and -bound enzymes fall on a single correlation line in the $\nu_{Fe\text{-}CO}$ versus ν_{CO} plot.(21) In contrast, the gsNOS data reported here demonstrate a more global conformational heterogeneity of the substrates-free enzyme, as the two $\nu_{Fe\text{-}CO}$-ν_{CO} data points fall on two distinct correlation lines, indicating differences on both the proximal and distal sides of the

heme in the two conformers (Fig. 5). Furthermore, substrate-binding in gsNOS not only introduces a positive electrostatic potential to the distal heme environment, but it also modulates the proximal Fe-Cys bond strength, as the Raman data indicate that the Fe-Cys bond in the NOHA-bound derivative is stronger than that in the L-Arg-bound enzyme. The transduction of the distal structural signal to the proximal side is plausibly mediated by the Trp70 residue, which π-stacks with the heme and donates an H-bond to the Cys, as discussed above. It is noteworthy that in P450cam, the binding of putidaredoxin has also been shown to change the strength of the proximal Fe-Cys bond, due to the modulation of its electrostatic environment. (46)

Although the exact mechanism for the substrate-binding induced perturbation in the proximal Fe-Cys moiety in gsNOS remains to be further investigated, the data reported here support mechanistic differences between the two steps of the NOS reaction in this bacterial enzyme. As such, it offers insights into the role of the proximal Cys→Fe electron donation in the oxygen chemistry of NOS. As illustrated in Scheme 2, one important factor leading to the two different mechanisms is that, in the L-Arg-bound enzyme, it is the terminal oxygen atom of the heme-bound dioxygen that accepts H-bonds from the substrate (L-Arg) and a water molecule, whereas in the NOHA-bound enzyme it is the proximal oxygen atom that accepts the H-bond from the substrate (NOHA).(32, 36, 37) The H-bonding to the distal oxygen atom in the L-Arg-bound enzyme facilitates the O-O bond cleavage, leading to the formation of the ferryl species that converts L-Arg to NOHA. In contrast, in the NOHA-bound enzyme, the H-bond donating from NOHA to the proximal oxygen atom inhibits the O-O bond cleavage; instead, it stabilizes the peroxyl species that inserts itself to NOHA via a nucleophilic addition reaction to generate citrulline and NO. The stronger Fe-Cys bond in the NOHA-bound derivative, as compared to the L-Arg-bound enzyme, revealed by the Raman data presented here indicates that the proximal Cys→Fe electron donation is stronger in the NOHA-bound enzyme. The increased “electronic push” from the proximal Cys ligand through the iron to the proximal oxygen atom plausibly strengthens its H-bond with NOHA, facilitating the second step of the NOS reaction.

CONCLUSIONS

We have shown that the CO-bound gsNOS from the thermophilic bacterium, *Geobacillus stearothermophilus*, exhibits two conformations in the absence of substrate, one with a stronger proximal Fe-Cys bond than the other. L-Arg stabilizes the conformer with the weaker Fe-Cys bond, whereas NOHA stabilizes the conformer with the stronger Fe-Cys bond, although both substrates introduce a positive electrostatic potential to the distal ligand binding site. The data indicate that substrate-binding in the distal pocket of gsNOS modulates both the distal and proximal heme environment, in contrast to mNOS, in which only the distal properties are affected. The unique modifications in the heme active site introduced by each substrate may be critical in defining the chemical environment required for carrying out the mechanistically distinct oxygen chemistry in each step of the NOS reaction.

Supplementary Material

Refer to Web version on PubMed Central for supplementary material.

Acknowledgments

This work was supported by grants from the NIH (GM054806 to DLR) and from the NSF (CHE-0749997 to BRC). MK is supported by the Medical Scientist Training Program at the Albert Einstein College of Medicine (NIH GM08572).

Abbreviations Used

5C, 6C	Five and six coordinated hemes, respectively
H4B	(6*R*)-5,6,7,8-tetrahydro-L-biopterin
NOHA	N-hydroxy-L-Arginine
NOS	Nitric oxide synthase
NOS_{oxy}	The oxygenase domain of nitric oxide synthase
eNOS, iNOS, nNOS	Endothelial, inducible, and neural mammalian nitric oxide synthases, respectively
mNOS	Mammalian nitric oxide synthase
bsNOS, gsNOS, saNOS	Nitric oxide synthases from the bacteria *Bacillus subtilis, Geobacillus stearothermophilus* and *Staphylococcus aureous*, respectively
ν_{Fe-CO}, ν_{C-O}, ν_{Fe-Cys}	The Fe-CO, C-O and Fe-Cys stretching modes, respectively
δ_{Fe-C-O}	The Fe-C-O bending mode

REFERENCES

1. Stuehr DJ. Biochim. Biophys.Acta. 1999; 1411:217–230. [PubMed: 10320659]
2. Siddhanta U, Presta A, Fan B, Wolan D, Rousseau DL, Stuehr DJ. J Biol Chem. 1998; 273:18950–18958. [PubMed: 9668073]
3. Panda K, Ghosh S, Stuehr DJ. J Biol Chem. 2001; 276:23349–23356. [PubMed: 11325964]
4. Crane BR, Arvai AS, Gachhui R, Wu C, Ghosh DK, Getzoff ED, Stuehr DJ, Tainer JA. Science. 1997; 278:425–431. [PubMed: 9334294]
5. Crane BR, Arvai AS, Ghosh DK, Wu C, Getzoff ED, Stuehr DJ, Tainer JA. Science. 1998; 279:2121–2126. [PubMed: 9516116]
6. Raman CS, Li H, Martasek P, Kral V, Masters BS, Poulos TL. Cell. 1998; 95:939–950. [PubMed: 9875848]
7. Li H, Raman CS, Glaser CB, Blasko E, Young TA, Parkinson JF, Whitlow M, Poulos TL. J. Biol. Chem. 1999; 274:21276–21284. [PubMed: 10409685]
8. Li H, Shimizu H, Flinspach M, Jamal J, Yang W, Xian M, Cai T, Wen EZ, Jia Q, Wang PG, Poulos TL. Biochemistry. 2002; 41:13868–13875. [PubMed: 12437343]
9. Fedorov R, Hartmann E, Ghosh DK, Schlichting I. J. Biol. Chem. 2003; 278:45818–45825. [PubMed: 12954642]
10. Chen PF, Tsai AL, Berka V, Wu KK. J Biol Chem. 1996; 271:14631–14635. [PubMed: 8663033]
11. Wang J, Stuehr DJ, Ikeda-Saito M, Rousseau DL. J. Biol. Chem. 1993; 268:22255–22258. [PubMed: 7693663]
12. Wang J, Stuehr DJ, Rousseau DL. Biochemistry. 1995; 34:7080–7087. [PubMed: 7539291]
13. Wang J, Stuehr DJ, Rousseau DL. Biochemistry. 1997; 36:4595–4606. [PubMed: 9109669]
14. Fan B, Wang J, Stuehr DJ, Rousseau DL. Biochemistry. 1997; 36:12660–12665. [PubMed: 9376373]
15. Tierney DL, Martasek P, Doan PE, Masters BSS, Hoffman BM. J. Am. Chem. Soc. 1998; 120:2983–2984.
16. Couture M, Adak S, Stuehr DJ, Rousseau DL. J Biol Chem. 2001; 276:38280–38288. [PubMed: 11479310]
17. Adak S, Crooks C, Wang Q, Crane BR, Tainer JA, Getzoff ED, Stuehr DJ. J Biol Chem. 1999; 274:26907–26911. [PubMed: 10480900]

18. Adak S, Wang Q, Stuehr DJ. J Biol Chem. 2000; 275:17434–17439. [PubMed: 10747960]
19. Adak S, Stuehr DJ. J Inorg Biochem. 2001; 83:301–308. [PubMed: 11293550]
20. Voegtle HL, Sono M, Adak S, Pond AE, Tomita T, Perera R, Goodin DB, Ikeda-Saito M, Stuehr DJ, Dawson JH. Biochemistry. 2003; 42:2475–2484. [PubMed: 12600215]
21. Rousseau DL, Li D, Couture M, Yeh SR. J Inorg Biochem. 2005; 99:306–323. [PubMed: 15598509]
22. Kers JA, Wach MJ, Krasnoff SB, Widom J, Cameron KD, Bukhalid RA, Gibson DM, Crane BR, Loria R. Nature. 2004; 429:79–82. [PubMed: 15129284]
23. Chen Y, Rosazza JP. J. Bacteriol. 1995; 177:5122–5128. [PubMed: 7545152]
24. Buddha MR, Keery KM, Crane BR. Proc. Natl. Acad. Sci. U.S.A. 2004; 101:15881–15886. [PubMed: 15520379]
25. Santolini J, Roman M, Steuhr DJ, Mattioli TA. Biochemistry. 2006; 45:1489–1489.
26. Salard I, Mercey E, Rekka E, Boucher JL, Nioche P, Mikula I, Martasek P, Raman CS, Mansuy D. J Inorg Biochem. 2006; 100:2024–2033. [PubMed: 17084900]
27. Chartier FJ, Couture M. Biophys. J. 2004; 87:1939–1950. [PubMed: 15345570]
28. Sudhamsu J, Crane BR. J Biol Chem. 2006; 281:9623–9632. [PubMed: 16407211]
29. Pant K, Bilwes AM, Adak S, Stuehr DJ, Crane BR. Biochemistry. 2002; 41:11071–11079. [PubMed: 12220171]
30. Bird LE, Ren J, Zhang J, Foxwell N, Hawkins AR, Charles IG, Stammers DK. Structure. 2002; 10:1687–1696. [PubMed: 12467576]
31. Crane BR, Rosenfeld RJ, Arvai AS, Ghosh DK, Ghosh S, Tainer JA, Stuehr DJ, Getzoff ED. Embo J. 1999; 18:6271–6281. [PubMed: 10562539]
32. Li D, Kabir M, Stuehr DJ, Rousseau DL, Yeh SR. J Am Chem Soc. 2007; 129:6943–6951. [PubMed: 17488012]
33. Rousseau, DL.; Li, D.; Hayden, EY.; Deng, H.; Yeh, SR. The Smallest Biomolecules: Diatomics and their Interactions with Hemeproteins. Ghosh, A., editor. Elsevier; Amsterdam: 2008. p. 465-497.
34. Griffith OW, Stuehr DJ. Annu Rev Physiol. 1995; 57:707–736. [PubMed: 7539994]
35. Pufahl RA, Wishnok JS, Marletta MA. Biochemistry. 1995; 34:1930–1941. [PubMed: 7531495]
36. Li H, Igarashi J, Jamal J, Yang W, Poulos TL. J Biol Inorg Chem. 2006; 11:753–768. [PubMed: 16804678]
37. Pant K, Crane BR. Biochemistry. 2006; 45:2537–2544. [PubMed: 16489746]
38. Li D, Stuehr DJ, Yeh SR, Rousseau DL. J Biol Chem. 2004; 279:26489–26499. [PubMed: 15066989]
39. Rousseau DL, Li D, Couture M, Yeh SR. J Inorg Biochem. 2005; 99:306–23. [PubMed: 15598509]
40. Yu, N-T.; Kerr, EA. Biological Applications of Raman Spectroscopy: Resonance Raman Spectra of Hemes and Metalloproteins. Spiro, TG., editor. Wiley; New York: 1987. p. 39-96.
41. Egawa T, Yeh SR. J Inorg Biochem. 2005; 99:72–96. [PubMed: 15598493]
42. Spiro TG, Wasbotten IH. J Inorg Biochem. 2005; 99:34–44. [PubMed: 15598489]
43. Xu C, Ibrahim M, Spiro TG. Biochemistry. 2008; 47:2379–2387. [PubMed: 18217776]
44. Bangcharoenpaurpong O, Champion PM, Martinis SA, Sligar SG. The Journal of Chemical Physics. 1987; 87:4273–4284.
45. Champion PM, Stallard BR, Wagner GC, Gunsalus IC. J. Am. Chem. Soc. 1982; 104:5469–5472.
46. Unno M, Christian JF, Sjodin T, Benson DE, Macdonald ID, Sligar SG, Champion PM. J Biol Chem. 2002; 277:2547–2553. [PubMed: 11706033]
47. Schelvis JP, Berka V, Babcock GT, Tsai AL. Biochemistry. 2002; 41:5695–5701. [PubMed: 11980473]
48. Dawson JH. Science. 1988; 240:433–439. [PubMed: 3358128]
49. Pant K, Crane BR. J Mol Biol. 2005; 352:932–940. [PubMed: 16126221]
50. Couture M, Stuehr DJ, Rousseau DL. Journal of Biological Chemistry. 2000; 275:3201–3205. [PubMed: 10652305]

51. Unno M, Christian JF, Benson DE, Gerber NC, Sligar SG, Champion PM. J. Am. Chem. Soc. 1997; 119:6614–6620.

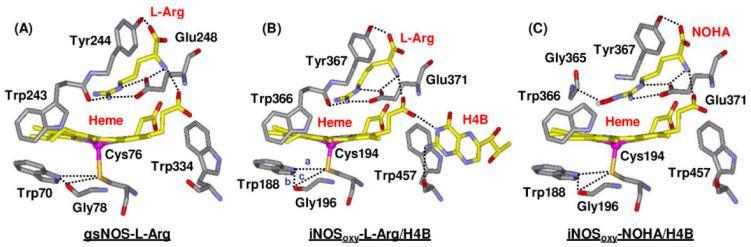

Fig. 1.

The catalytic site of (A) L-Arg-bound gsNOS (2FLQ), (B) L-Arg-bound iNOSoxy (1NOD) and (C) NOHA-bound iNOSoxy (1DWX). In (B) and (C), H4B is also present in the crystal structures, but not shown in (C) for clarity. The H-bonding interactions are indicated by the dashed lines. The distances indicated in (B) by (a, b and c) in the proximal side of each heme are listed in Table 2.

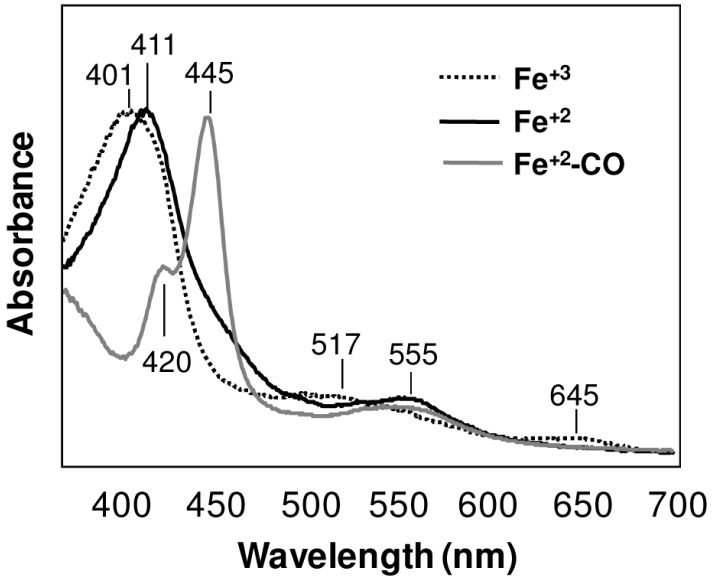

Fig. 2.
Optical absorption spectra of the ferric (dotted line), ferrous (solid black line) and CO-bound ferrous (solid grey line) forms of gsNOS in the absence of substrates and cofactor.

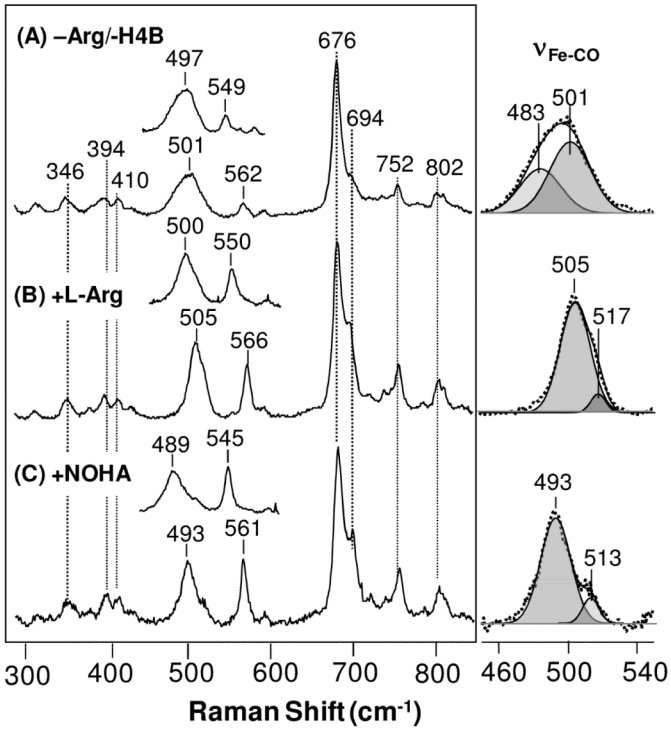

Fig. 3.

Resonance Raman spectra of $^{12}C^{16}O$-bound gsNOS in the absence of substrates and cofactor (A), in the presence of L-arginine (B) and in the presence of NOHA (C). The insets above each spectrum show the spectra of the same derivatives obtained with $^{13}C^{16}O$-bound gsNOS. Right panel: the best fit of each Fe-CO stretching mode with two Gaussian curves as indicated by the shaded areas. All the parameters were allowed to fee-float in the fitting routine. The dotted lines are the experimental data and the solid lines are the fits.

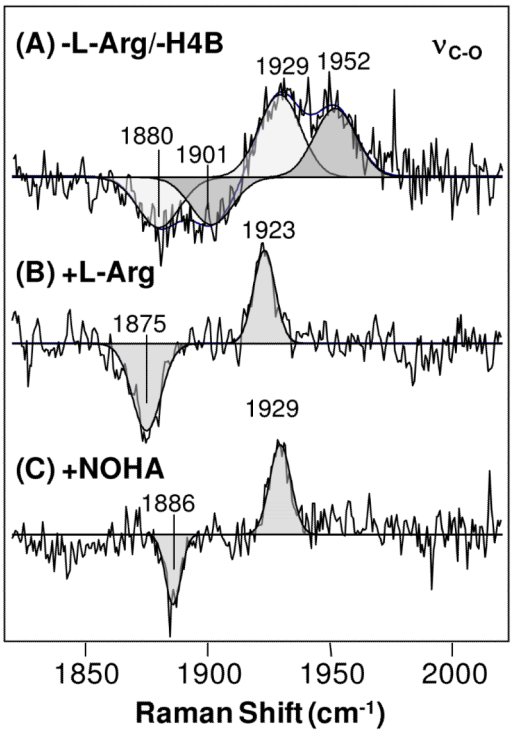

Fig. 4.

Resonance Raman isotope difference spectra ($^{12}C^{16}O$-$^{13}C^{16}O$) for the C-O stretching modes of CO-bound gsNOS in the absence of substrates and cofactor (A), in the presence of L-Arg (B) and in the presence of NOHA (C). Each difference spectrum was fitted with two Gaussian curves for the positive bands and two Gaussian curves for the negative bands, with procedures as described in Fig. 3. As the signal in this region is very weak, the difference spectra, instead of the original spectra, were analyzed.

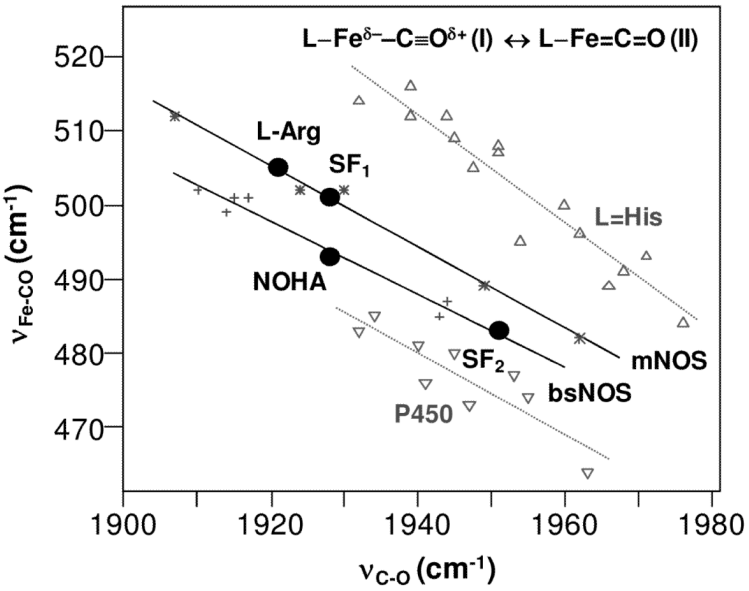

Fig. 5.

The ν_{CO}-ν_{Fe-CO} inverse correlation plot of the CO derivatives of hemeproteins with a proximal ligand of histidine (Δ), the mNOS enzyme family (*), the bsNOS enzyme (+) and P450 enzyme family (∇). The data indicated as SF1 and SF2 are those associated with the substrate-free gsNOS. The data indicated as L-Arg and NOHA are those associated with L-Arg and NOHA-bound gsNOS, respectively. The data points for gsNOS (black circles) fall on two different correlation lines. All points other than those from gsNOS were taken from prior reports.(40-42)

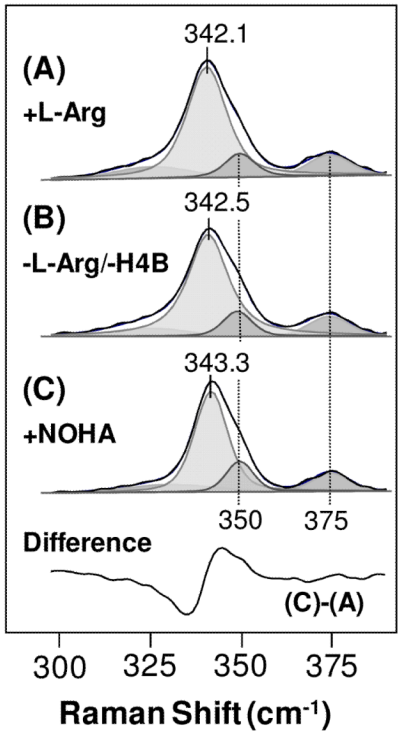

Fig. 6.

The Fe-Cys stretching modes of the various derivatives of gsNOS as indicated. The bottom trace shows the difference spectrum of (C)-(A). Each mode was fitted with a Gaussian/Lorentzian mixture, with all the parameters free-floating. The lines at 350 and 375 cm^{-1} are assigned as porphyrin modes.

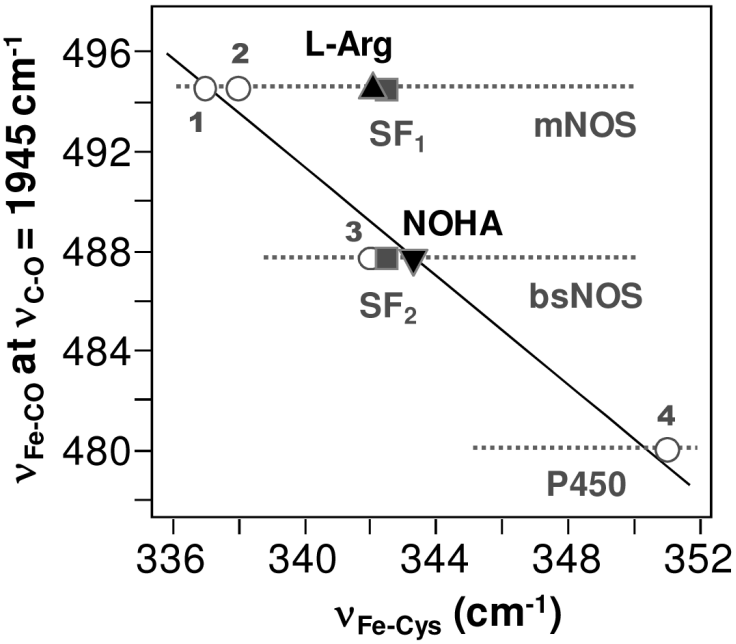

Fig 7.

A plot of the offset of the ν_{CO}-$\nu_{Fe\text{-}CO}$ inverse correlation line shown in Fig. 5 as a function of the $\nu_{Fe\text{-}Cys}$ frequency. The offsets of the inverse correlation lines are taken from the y-intercept in Fig. 5, defined by the $\nu_{Fe\text{-}CO}$ frequency at $\nu_{C\text{-}O}$ =1945 cm^{-1}. The data points 1 and 2 are from mNOS(25, 47), while the data points 3 and 4 are from bsNOS(25) and P450 in the absence of Putaredoxin(45, 51), respectively. The solid squares, indicated as SF1 and SF2, are associated with the two data points of the substrate-free gsNOS. The up and sown triangles are associated with the L-Arg and NOHA-bound gsNOS, respectively.

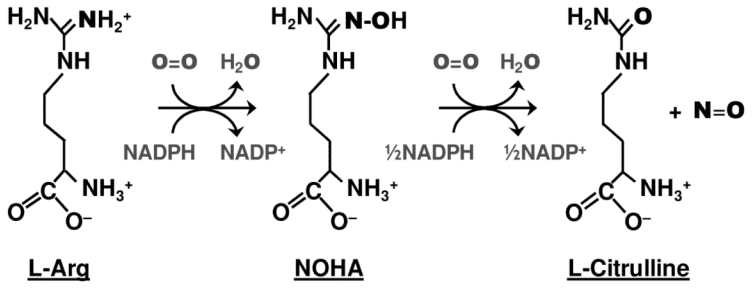

Scheme 1.

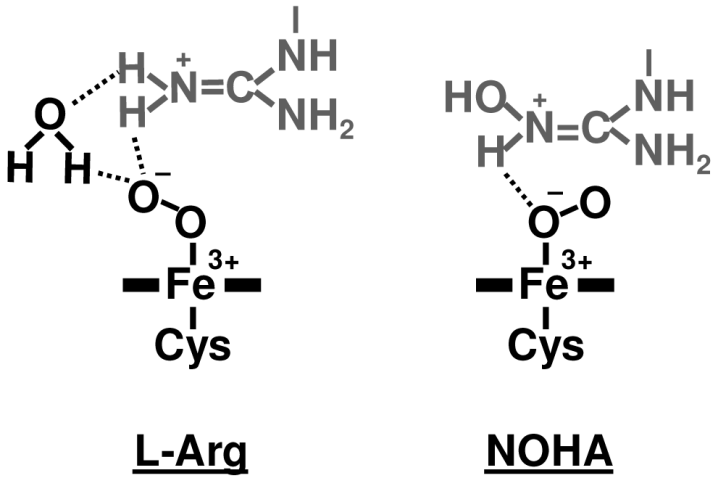

L-Arg NOHA

Scheme 2.

Table 1

The various heme ligand-related vibrational frequencies (cm^{-1}) in gsNOS as compared to other NOSs

The relative intensities of the multiple $\nu_{Fe\text{-}CO}$ and $\nu_{C\text{-}O}$ modes are indicated as w (weak), m (medium) and s (strong).

NOS		$\nu_{Fe\text{-}CO}$	$\nu_{C\text{-}O}$	$\delta_{Fe\text{-}C\text{-}O}$	$\nu_{Fe\text{-}Cys}$	REF
gsNOS	S-Free±H4B	483(m),501(m)	1952(m),1929(m)	562	342.5	This work
	L-Arg±H4B	505(s),517(w)	1923	566	342.1	
	NOHA±H4B	493(s),513(w)	1929	561	343.3	
bsNOS	S-Free	485(m),499(m)	1943(s),1914(w)	564		(25)
	L-Arg	502	1910	568		
	H4B	487(m),501(s)	1944(m),1933(m), 1917(m)			
	L-Arg±H4B	501	1915	567	342	
saNOS	S-Free	482(m),497(m)	1949(m),1930(m)	560		(27)
	L-Arg±H4B	504	1917	566		
iNOSoxy	S-Free±H4B	482(m),502(m)	1945(broad)	562		(32, 33, 38)
	L-Arg±H4B	482(w),502(m), 512(s)	1907	569	337	(25, 32, 33, 38)
	NOHA±H4B	482(m),500(s), 512(w)	1930(m),1904(w)	562		(32, 33, 38)
nNOSoxy	S-Free±H4B	489(s),501(w), 514(w)		562		(32, 33, 50)
	L-Arg±H4B	489(m),502(m), 514(m)	1932	565		
	NOHA±H4B	490(m),501(m), 514(w)		562		

Table 2

The distances between the three critical proximal amino acids in the crystallographic structure of each subunit of various NOSs

The distances, S_{Cys}-N_{Trp}, N_{Trp}-O_{Gly} and O_{Gly}- S_{Cys}, are defined as a, b and c, respectively, in Fig. 1B, which correspond to the distances between the sulfur atom of the proximal cysteine and the nitrogen atom of the nearby tryptophan (a), the nitrogen atom of the tryptophan and the backbone oxygen atom of the nearby glycine (b), and the oxygen atom of the glycine and the sulfur atom of the proximal cysteine (c).

NOS	PDB	Subunit A			Subunit B		
		S*Cys*-N*Trp*	N*Trp*-O*Gly*	O*Gly*-S*Cys*	S*Cys*-N*Trp*	O*Gly*-N*Trp*	O*Gly*-S*Cys*
eNOS*oxy* (+Arg)	4NSE	3.38	4.37	4.81	3.32	4.19	4.82
nNOS*oxy* (+Arg+H4B)	1OM4	3.44	4.44	4.85	3.49	4.31	4.86
iNOS*oxy* (+Arg+H4B)	1NOD	3.22	4.71	5.08	3.23	4.39	4.83
iNOS*oxy* (+NOHA,+H4B)	1DWX	3.15	4.69	5.02	3.14	4.41	4.74
saNOS	1MJT	3.29	3.97	4.46	3.36	4.03	4.45
bsNOS	2AMO	3.74	4.31	4.86	3.40	3.77	4.49
bsNOS (+Arg+THF	1M7V	3.47	4.04	4.80			
bsNOS (+NOHA+THF)	1M7Z	3.48	4.01	4.80			
gsNOS	2FLQ	3.73	3.07	3.89	3.74	3.61	3.90